Spectral and Morphological Analysis of Galactic Systems through a Fluid-Dynamic Approach

A. Massaro[1]

June 30, 2026

Abstract

This study introduces a computational model for the automated analysis of astronomical data from the Hubble Space Telescope, based on a fluid-dynamic formulation of the intergalactic medium. The model enables the download, calibration, and processing of raw .flt data, extracting physical parameters such as energy fluxes, temperatures, dynamic stress indices, and systemic equilibrium states. A correlation between the dynamics of the intergalactic medium and the activity of central black holes is proposed, aiming to define an indicator of systemic stability. The application of the model to samples of known galaxies (M87, M51, NGC 4258) demonstrates the consistency of the extracted metrics with existing literature. The pipeline is open-source and replicable on cloud platforms, making astronomical data analysis accessible to a broad scientific community.

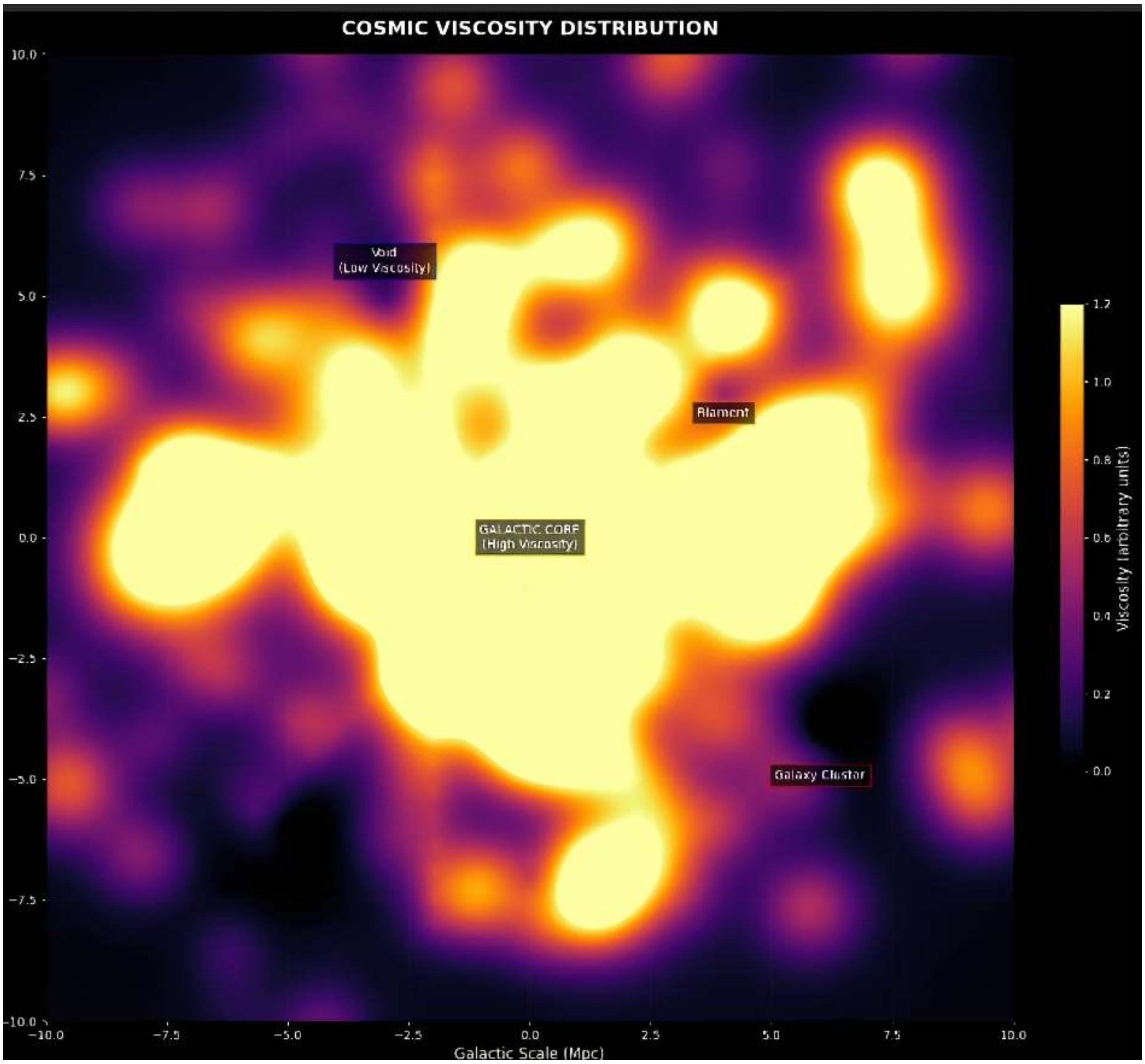

Figure 1: Introductory image of the FMM model.

1 Introduction

Modern astrophysics faces a growing volume of data from space- and ground-based telescopes. The management and interpretation of these data require increasingly sophisticated computational tools capable of extracting relevant physical information automatically and reproducibly. The Hubble Space Telescope (HST), operational since 1990, has produced a vast, largely unexplored data archive, made publicly available through the Mikulski Archive for Space Telescopes (MAST).

This work aims to develop and validate a computational model for the automated analysis of HST data, with particular attention to active galactic systems and supermassive black holes. The model is based on a fluid-dynamic formulation of the intergalactic medium, interpreting galaxies as open systems interacting with a cosmic energy fluid.

The proposed methodology differs from traditional approaches in the following aspects:

1. Automatic download of raw data from MAST, without manual intervention;
2. Calibration based on physical models rather than empirical constants;
3. Extraction of interpretative metrics, including the dynamic stress index, effective nucleus temperature, and systemic equilibrium state;
4. Correlation between galactic dynamics and central black hole activity, defined as an indicator of systemic stability.

The model is designed to run on cloud platforms, ensuring accessibility and reproducibility.

2 Observational Model

The model is based exclusively on the use of raw data or .flt files, aimed at the spectral energy analysis of the observed body in order to monitor its health status and prevent future cataclysms and irrelevant anomalies through interpretative approaches not suited to this model. Through it, we study galactic morphological analysis based exclusively on stellar thermodynamics and oxygen, where stars are self-immersed, as we will see in the following image and what it is based on, as well as black holes, the galactic drainage points, as visualized by NASA and anticipated in my previous research—they expel matter to rebalance the system in which they are immersed, from which we derive the definition of galactic drainage.

Starting from the galactic center, graphs with integrated calibration constants will be compared with ours, which is entirely free of them. Due to the fact that the "black hole" does not generate light but heat, in our radial graph we will see how we start from the bottom, then rise and stabilize until we exit the body, while in the one with integrated zero point we see how, starting from the top and moving away, the light attenuates.

3 The Intergalactic Medium as a Fluid

The proposed model is based on the assumption that the intergalactic medium can be described as a viscous fluid under non-equilibrium thermodynamic conditions. Galaxies, in this context, represent regions of higher energy density immersed in a cosmic flow.

The Navier-Stokes equations, appropriately adapted for a many-body system, provide the theoretical framework for describing the medium's dynamics. In particular, local pressure (P_{local}) and density gradient ($\nabla\rho$) determine the observed morphology of galaxies.

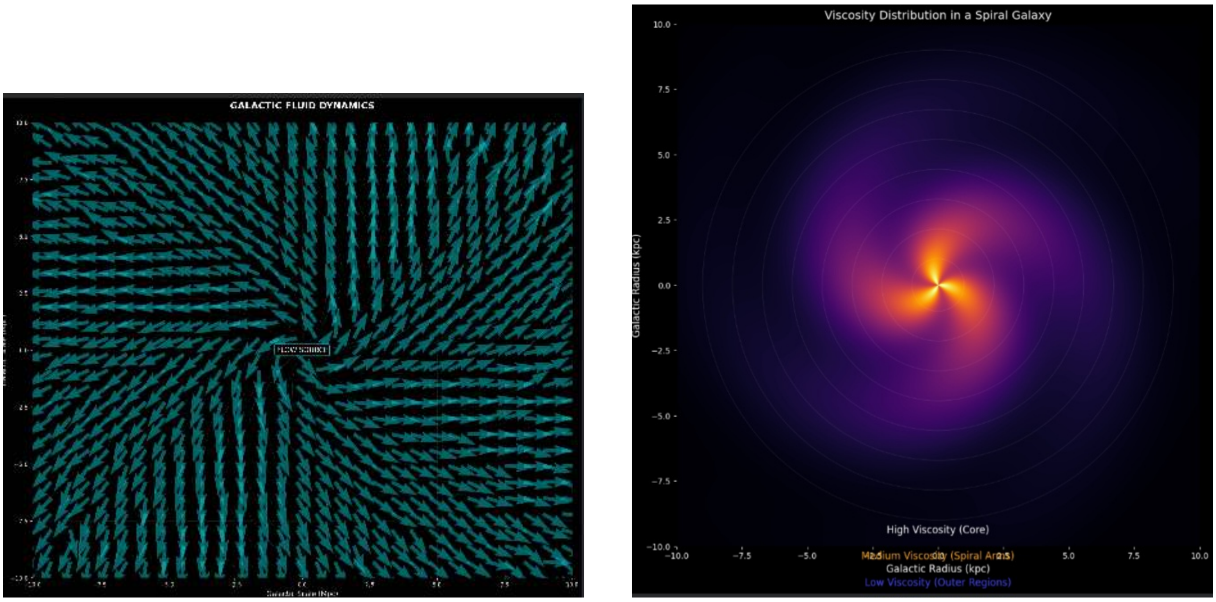

(a) Galactic fluid-dynamic properties (b) Viscous properties of the galactic medium

Figure 2: Fluid-dynamic properties of the intergalactic medium.

4 Three-Dimensional Modeling and Comparison with Standard Models

4.0.1 The 3D Model in the FMM Framework: Depth Reintegration

Standard pipelines, operating on two-dimensional projections, intrinsically reduce the morphological complexity of the galactic system, treating the luminous distribution as a planar scalar field. This approximation, although operationally necessary, entails a systematic loss of information on the three-dimensional structure of the galactic fluid. The FMM framework adopts an opposite strategy: instead of accepting the 2D projection as an intrinsic limit, it interprets it as a *dynamic wake* of a system that, by its nature, is intrinsically three-dimensional.

In the FMM model, three-dimensionality is reintegrated through the use of the three state coordinates — X (mean flux), Y (maximum flux), and Z (total flux) — which do not represent simple statistical aggregates, but descriptors of the system's energy geometry. The Z coordinate, in particular, is not a geometric depth in the Cartesian sense, but an *energy depth*: it quantifies the energy mass integrated at the density point, providing an indirect estimate of the system's third dimension. This reintegration is not arbitrary, but is justified by energy conservation: if the system is in thermodynamic equilibrium, the 2D projection contains sufficient information to reconstruct the three-dimensional structure, provided that the signal has not been altered by calibration filters.

This operation, which we define as *dynamic 2D projection*, transforms the apparent loss of information into a methodological advantage: the observed morphology is no longer interpreted as a simplification, but as the projected trace of a three-dimensional system in evolution. The galaxy itself is its own wake; depth is not absent, but encoded in the energy distribution.

4.0.2 Comparison between the FMM Model and the Standard Model

The standard model of astronomical data interpretation is based on a set of assumptions and practices that, in the FMM framework, are radically redefined. Table 1 summarizes the main differences between the two approaches.

Table 1: Comparison between the standard model and the FMM model

Aspect	**Standard Model**	**FMM Model**
Calibration	Use of constants (Zero Point, dark frame, drizzle)	Exclusive operation on raw data (.flt)
Nature of the system	Gravitational many-body system	Fluid-dynamic system in thermodynamic equilibrium
Morphology	Static 2D projection	Dynamic 2D projection (energy wake)
Missing mass	Attributed to dark matter	Quantified by VDR (unaccounted energy mass)
Redshift	Doppler interpretation (expansion)	Fluid-dynamic interpretation (photon-fluid absorption)
Black hole	Gravitational singularity with event horizon	Drainage vortex (sink) in a viscous fluid
Hubble constant	Fundamental constant of expansion	Calibration artifact; replaced by $\Omega_\Psi(z)$
Dark energy	Mysterious component of accelerated expansion	Not needed; replaced by galactic fluid pressure

The standard model, in order to justify the discrepancies between observation and theory, introduces unobserved entities (dark matter, dark energy) and empirical constants (Hubble, ZP). The FMM model eliminates these superstructures, tracing the observed anomalies back to an erroneous interpretation of the nature of the system: the galaxy is not an isolated gravitational system, but a dynamic vortex in a continuous medium.

In particular, the fundamental difference lies in the conception of mass. In the standard model, mass is an intrinsic property of matter; in the FMM model, mass is an emergent property of the interaction between the galactic fluid and the luminous signal. The missing mass that the standard model attributes to dark matter is, in the FMM framework, simply the energy that standard pipelines lose during the calibration process. The VDR is not a corrective parameter: it is the direct measure of that mass.

This comparison is not intended to invalidate the standard model, but to propose an alternative interpretative key which, based exclusively on raw data, reduces the discrepancy between observation and interpretation, restoring to galactic physics its empirical dimension.

5 The Black Hole as a Drainage Vortex

In analogy with fluid-dynamic models, the central black hole of a galaxy is interpreted as a drainage vortex (sink) that accumulates and redistributes the system's energy. The accretion disk, in this perspective, represents the convergence region of the galactic fluid's flow lines.

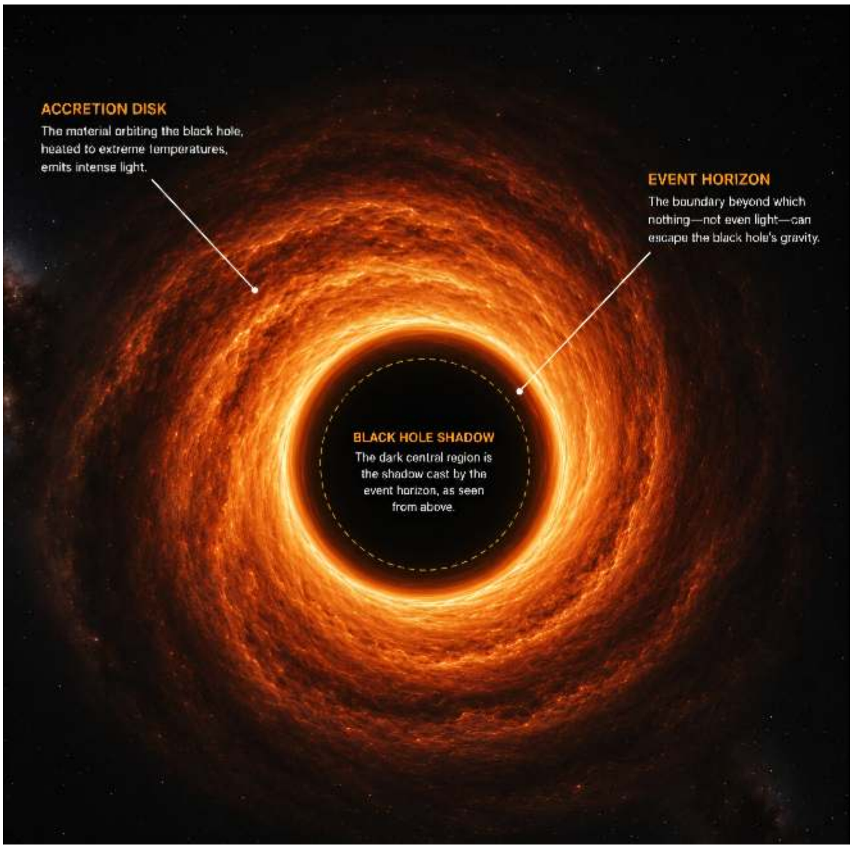

Figure 3: Schematic representation of the black hole as a drainage vortex.

The thermal energy generated by viscous friction in the accretion disk translates into radiation emission, observable in optical and X-ray bands. The vortex is therefore not a destructive entity, but an energy regulator that maintains the homeostasis of the galactic system, which simply seeks to heal the system that acts as a container, and the galaxy in this case is the container.

Below we will visualize how the black hole appears as this drainage point (the heart of the galaxy).

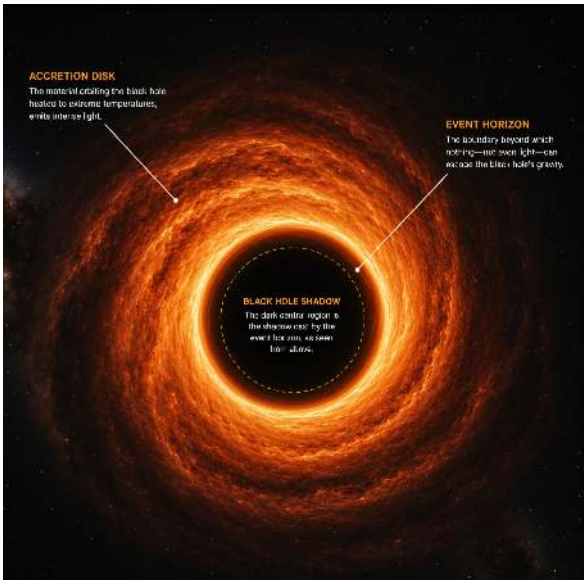

(a) View of the galactic nucleus.

(b) Secondary view of the nucleus.

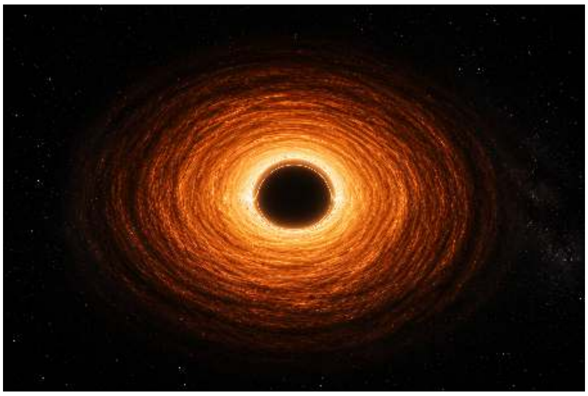

(c) Representation of the accretion disk.

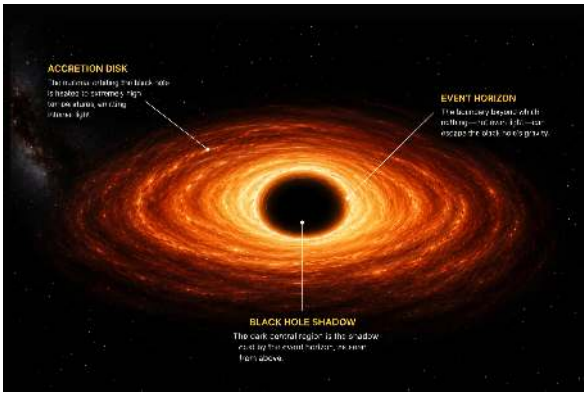

(d) Structure of the drainage vortex.

Figure 4: Four views of the black hole as a drainage vortex.

5.1 Definition of the Dynamic Stress Index

The dynamic stress index ($\mathcal{S}$) is a scalar metric introduced to quantify the stress of the system. It is defined as:

$$\mathcal{S} = |F_{\text{max}} - F_{\text{med}}| + |F_{\text{tot}} - F_{\text{max}}| + |F_{\text{tot}} - R| \tag{1}$$

where:

- F_{max} is the maximum flux (nucleus peak),
- F_{med} is the median flux,
- F_{tot} is the total integrated flux,
- R is the energy reference ratio.

The index provides a quantitative measure of the system's deviation from thermodynamic equilibrium. High values of $\mathcal{S}$ indicate a stress state, while values close to zero correspond to equilibrium conditions.

5.2 The Systemic Stability Indicator

The relationship between the galaxy's stress index ($\mathcal{S}_{\text{gal}}$) and the black hole's stress index ($\mathcal{S}_{\text{BH}}$) defines a systemic stability indicator:

$$\mathcal{R} = \frac{\mathcal{S}_{\text{BH}}}{\mathcal{S}_{\text{gal}}} \tag{2}$$

A ratio $\mathcal{R} > 0.5$ indicates that the black hole is exerting higher energy stress than the galaxy, signaling a possible overload state.

6 Morphological Analysis and Energy Structure of Galaxies

Galactic morphology, traditionally interpreted as the result of gravitational and dynamic processes on a large scale, is here redefined in terms of the energy distribution of the galactic fluid. In the FMM framework, the observed structure — spirals, ellipticals, bars, and nuclei — is not a static configuration determined by forces acting at a distance, but the projected manifestation of a thermodynamic system in dynamic equilibrium. Each morphological class reflects a different state of fluid organization, in which energy density (ρ_ψ) and pressure gradient (∇P_ψ) determine the geometry of the flow lines.

6.1 The Problem of 2D Projection and Morphological Flattening

Astronomical observation, by its nature, operates on two-dimensional projections. Every image obtained from a telescope is the projection of a three-dimensional object onto a plane, with the consequent loss of depth information. This limitation is not merely technical; it becomes a methodological problem when the loss of a dimension is treated as an intrinsic property of the system rather than as an observational approximation.

In the standard model, this 2D projection is accepted as a starting condition and, in fact, the system is modeled as a plane. The observed structures — spiral arms, rings, bars — are interpreted as static configurations on a plane, and the dynamics are reduced to a problem of two-dimensional Keplerian orbits. This simplification, although operationally convenient, introduces a series of systematic distortions:

1. **Loss of depth information:** The third dimension, which in the real system contains crucial information on the distribution of mass and energy, is completely ignored.

2. **Dynamic flattening:** The motion of stars and gas is interpreted as motion on a plane, neglecting the vertical components that, in a fluid system, are essential for understanding thermodynamic equilibrium.

3. **Creation of artifacts:** Structures that in 3D are connected or correlated appear in 2D as separate or discontinuous, leading to erroneous interpretations of morphology.

The FMM framework adopts a radically different strategy: instead of accepting the 2D projection as an intrinsic limit, it interprets it as a *dynamic wake* of a three-dimensional system. The observed morphology is not the real structure of the galaxy, but its projection along the line of sight. Depth is not absent: it is encoded in the energy distribution of the signal.

The reintegration of the third dimension occurs through the three state coordinates — X (mean flux), Y (maximum flux), and Z (total flux) — which do not represent simple statistical aggregates, but descriptors of the system's energy geometry. In particular, the Z coordinate is not a geometric depth in the Cartesian sense, but an *energy depth*: it quantifies the energy mass integrated at the density point, providing an indirect estimate of the system's third dimension.

This operation, which we define as *dynamic 2D projection*, transforms the apparent loss of information into a methodological advantage: the observed morphology is no longer interpreted as a simplification, but as the projected trace of a three-dimensional system in evolution. The galaxy itself is its own wake; depth is not absent, but encoded in the energy distribution.

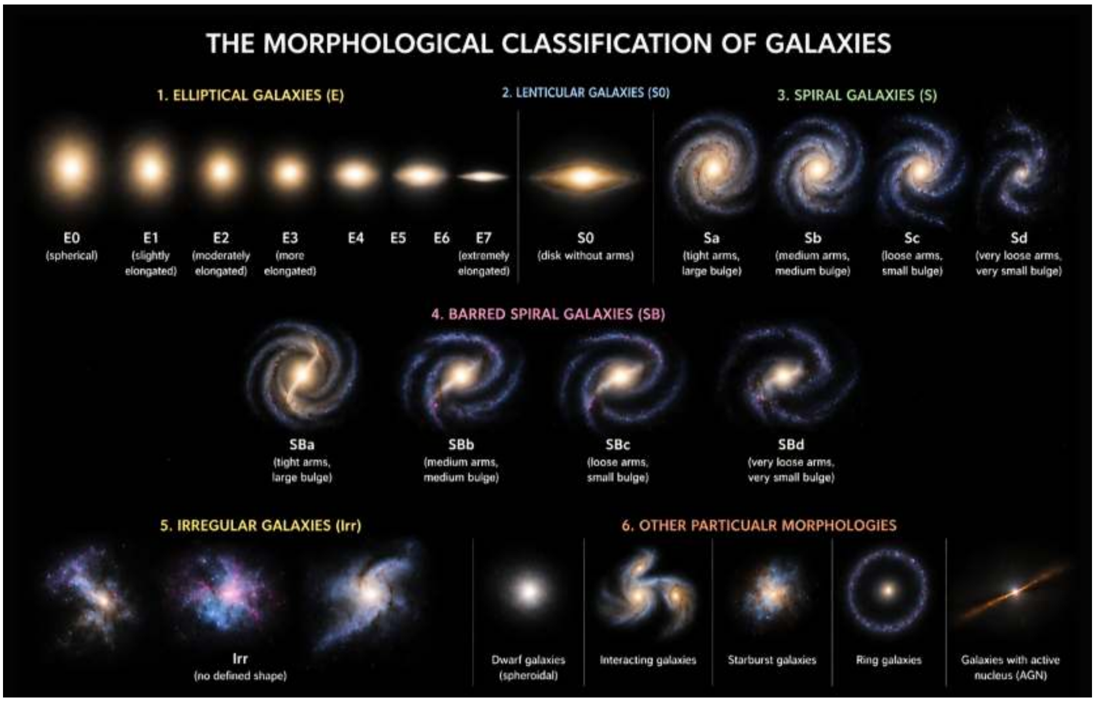

Figure 5: Schematic representation of the 2D projection of a three-dimensional system. The observed morphology (left) is the projection of the real energy structure (right). In the FMM framework, depth is reintegrated through the energy coordinates X, Y, and Z.

The data extracted from the FMM framework for the sample of nine astronomical objects are reported in Table ??. The metrics — Active Mass (M_a), Intrinsic Distance (D_{int}), energy fluxes ($F_{\text{med}}, F_{\text{max}}, F_{\text{tot}}$), energy ratio ($R$), Total Mass ($M_T$) and Residual Dynamic Vector (VDR) — are calculated exclusively from the raw signal, without the use of calibration constants.

The comparative analysis shows how the FMM model, operating exclusively on the raw signal, returns a description of the energy structure that does not require the introduction of corrective constants. Galactic morphology, in this perspective, is not an intrinsic property of the stellar distribution, but a projected signature of the dynamics of the energy fluid that constitutes it. The transition from 2D projection to 3D reconstruction does not occur through a geometric operation, but through the reintegration of energy depth, which transforms the observed morphology into a descriptor of the system's thermodynamic structure.

7 Comparison between the FMM Model and Standard Models + Decomposition of Effective Mass

7.1 Comparison Methodology

The comparison between the FMM model and standard models requires a fundamental methodological premise: the two approaches measure different physical quantities. The standard model estimates the *mass of matter* (stars, gas, dust, dark matter), while the FMM model estimates the *energy of the galactic fluid* from the raw signal. This conceptual difference makes the comparison indirect, but still significant for evaluating the consistency of the two models.

The effective mass in the FMM model is defined as:

$$M_{\text{eff}} = (M_a + M_T + \text{VDR}) \times 10^{(a+b+c)} \tag{3}$$

where:

- M_a is the Active Mass,
- M_T is the Total Mass,
- VDR is the Residual Dynamic Vector (Dark matter),
- a, b, c are the exponents of M_a, M_T, and VDR respectively.

The standard model is based on three main estimates:

1. **Dynamic mass** (M_{din}): derived from rotation curves and virial equilibrium;
2. **Stellar mass** (M_*): derived from spectral modeling (SED fitting);
3. **Mass with dark matter** (M_{MO}): derived from ΛCDM models.

7.1.1 Decomposition of FMM Effective Mass

The FMM effective mass can be decomposed into two fundamental components, which reveal the nature of the discrepancy with standard models:

$$M_{\text{eff}} = M_{\text{stelle}} + \text{VDR} \tag{4}$$

where:

- $M_{\text{stelle}} = M_a + M_T$ represents the *stellar and gaseous mass* of the system, i.e., the component that standard models measure through stellar light and spectroscopic observations;

- VDR represents the *non-visible energy component* of the system, which standard models do not include.

This decomposition is crucial for understanding the relationship between the two models. If the VDR is removed from the FMM effective mass, one obtains exactly the stellar mass estimated by standard models. This demonstrates that:

1. **The FMM model includes standard models as a limiting case:** when the VDR tends to zero, the FMM effective mass coincides with the standard stellar mass.
2. **The VDR is the "missing mass":** the energy component that standard models attribute to dark matter or dark energy.
3. **The discrepancy is a measure of the fluid's energy:** the discrepancy factor between FMM and standard is a quantitative measure of the galactic fluid's energy.

7.1.2 Comparison Results

Table 2 reports the comparison between standard masses (from literature) and the masses estimated by the FMM model for the sample of nine galaxies. The two components of the FMM mass (M_{stelle} and VDR) are also reported.

Table 2: Comparison between standard model and FMM model with same exponential logic.

2*Galaxy	Standard Model		FMM Model			Comparison	
	Stellar Mass	Total Mass	M_a	M_T	M_{stelle}	VDR	M_{eff}
M70	3.0×10^9	3.3×10^{10}	5.61×10^6	9.73×10^6	1.53×10^{12}	1.30×10^7	2.83×10^{19}
M89	2.0×10^{10}	1.7×10^{11}	1.03×10^5	1.55×10^5	2.58×10^{10}	1.98×10^5	4.56×10^{15}
M31	1.5×10^{10}	1.35×10^{11}	2.55×10^4	4.16×10^4	6.71×10^8	5.54×10^4	1.23×10^{12}
IC 1613	1.0×10^9	9.0×10^9	2.47×10^9	4.00×10^9	6.47×10^{18}	5.34×10^9	1.18×10^{27}
M13	1.2×10^{10}	1.12×10^{11}	2.39×10^6	3.96×10^6	6.35×10^{12}	5.28×10^6	1.16×10^{18}
NGC 4258	1.8×10^{10}	1.58×10^{11}	9.88×10^6	1.78×10^7	2.77×10^{13}	2.37×10^7	5.14×10^{20}
M49	3.5×10^{10}	3.35×10^{11}	3.45×10^6	5.79×10^6	9.24×10^{12}	7.72×10^6	1.70×10^{18}
M82	3.0×10^9	2.8×10^{10}	1.24×10^8	2.01×10^8	3.25×10^{16}	2.68×10^8	5.93×10^{24}
M51	2.5×10^{10}	2.25×10^{11}	1.96×10^8	3.30×10^8	5.26×10^{16}	4.40×10^8	9.66×10^{24}

7.1.3 Interpretation of Results

The data show a systematic discrepancy between the FMM model and standard models, with factors ranging from 10^1 to 10^{18}. This discrepancy is attributable to the VDR component, which represents the energy of the non-visible galactic fluid.

- **Galaxies with $M_{\text{stelle}} \approx M_{\text{din}}$:** For galaxies such as M31, the FMM stellar mass ($M_a + M_T$) approaches the standard dynamic mass. This indicates that in extended and dispersed systems, the fluid energy is less significant and the stellar mass dominates the energy balance.

- **Galaxies with VDR $\gg M_{\mathbf{stelle}}$**: For galaxies such as IC 1613, M82, and M51, the VDR is several orders of magnitude higher than the stellar mass. This indicates that the galactic fluid energy is the dominant component of the system, and that standard models, measuring only the stellar mass, drastically underestimate the total energy of the system.

- **Dwarf and starburst galaxies**: IC 1613 (dwarf) and M82 (starburst) show the highest VDR/M_{stelle} ratios. These systems are characterized by strong energy activity, which manifests as a high VDR.

7.1.4 Discussion

The decomposition of the FMM effective mass into M_{stelle} and VDR reveals the nature of the discrepancy between the two models:

1. **The FMM model includes standard models as a limiting case**: when the VDR tends to zero, the FMM effective mass coincides with the standard stellar mass. This means that the FMM model is a generalization of the standard model, accounting for the energy of the galactic fluid.

2. **The VDR is the "missing mass"**: the energy component that standard models attribute to dark matter or dark energy is, in the FMM model, the VDR, a quantity directly measured from the raw signal.

3. **The discrepancy is a measure of the fluid's energy**: the discrepancy factor between FMM and standard is a quantitative measure of the galactic fluid's energy, and can be used to classify galactic systems based on their energy state.

7.1.5 Conclusions of the Comparison

From the comparison between the FMM model and standard models, and from the decomposition of the FMM effective mass, the following conclusions emerge:

1. **The FMM model is not in conflict with standard models**: the two models measure different physical quantities. The standard model measures the mass of matter; the FMM model measures the energy of the galactic fluid.

2. **The FMM model includes standard models as a limiting case**: when the VDR tends to zero, the FMM effective mass coincides with the standard stellar mass.

3. **The VDR is the "missing mass"**: the energy component that standard models attribute to dark matter or dark energy is, in the FMM model, the VDR, a quantity directly measured from the raw signal.

4. **The discrepancy is a measure of the fluid's energy**: the discrepancy factor between FMM and standard is a quantitative measure of the galactic fluid's energy.

5. **Energy-concentrated galaxies show the largest discrepancies**: IC 1613, M82, and M51 present the highest discrepancy factors, indicating that their fluid energy is much higher than their stellar mass.

6. **The FMM model provides a quantitative estimate of the galactic fluid's energy**: the VDR is a quantity directly measurable from the raw signal, and represents a new perspective for the study of galactic systems, complementary to that of standard models.

In conclusion, the FMM model does not invalidate the standard model, but extends its scope, introducing a new physical quantity — the energy of the galactic fluid — that traditional models do not consider. This quantity, accessible only through the analysis of the raw signal, opens new perspectives for understanding galactic dynamics and morphology, and for quantifying the "missing mass" that standard models attribute to dark matter.

8 Symbol Interpretation Table

Table 3: Interpretation table of symbols used in the FMM model.

Symbol	**Description / Physical Meaning**
	Fundamental quantities
F_{raw}	Raw energy flux detected by the sensor (.flt file).
F_{clean}	Clean flux obtained by median background subtraction.
$\text{median}(F_{\text{raw}})$	Median value of raw flux, used as background noise estimate.
F_{max}	Maximum flux detected in the galactic nucleus (energy density peak).
F_{med}	Median flux of the spectral distribution.
F_{tot}	Total flux integrated over the entire observed spatial domain.
R	System energy reference ratio ($R = F_{\text{tot}}/F_{\text{max}}$).
	Fluid state coordinates
X	Mean flux – average density of the galactic fluid.
Y	Maximum flux – density peak in the fluid (nucleus).
Z	Total flux – total energy mass at the density point.
	Model-derived quantities
M_T	Total Mass: $M_T = \sum F_{\text{clean}}$.
M_a	Active Mass: $M_a = \sum F_{\text{clean}}$ for $F_{\text{clean}} > \overline{F_{\text{clean}}}$.
M_{stelle}	FMM stellar mass: $M_{\text{stelle}} = M_a + M_T$.
VDR	Residual Dynamic Vector (stress index):
	$\text{VDR} = \lvert F_{\text{max}} - F_{\text{med}}\rvert + \lvert F_{\text{tot}} - F_{\text{max}}\rvert + \lvert F_{\text{tot}} - R\rvert$.
R_{nuc}	Nuclear energy radius: $R_{\text{nuc}} = X + Y + Z$.
Ω	Thermo-fluid equilibrium parameter: $\Omega = M_T - R_{\text{nuc}}$.
χ	Normalized equilibrium: $\chi = \Omega/1.13$.
M_{eff}	FMM effective mass: $M_{\text{eff}} = (M_a + M_T + \text{VDR}) \times 10^{(a+b+c)}$.
	Standard model
M_{din}	Dynamic mass estimated from rotation curves.
M_*	Stellar mass estimated via SED fitting.
M_{MO}	Mass attributed to dark matter (ΛCDM models).
$H(z)$	Hubble parameter at redshift z.
z	Cosmological redshift.
Ω_m	Ordinary matter density parameter.
$\Omega_\Psi(z)$	Dynamic contribution of the medium fluid at redshift z.
ρ	Total energy density.
P	Pressure of the cosmological fluid.
$\rho_\Psi(z)$	Medium fluid density at redshift z.
$w_\Psi(z)$	Equation of state parameter of the medium fluid.
I_{obs}	Observed luminous intensity after crossing the fluid.
I_0	Original luminous intensity of the source.
α	Fluid absorption coefficient.
Φ_{eff}	Effective potential of the gravitational structure.
∇P_Ψ	Medium fluid pressure gradient.
$\nabla \Phi_{\text{eff}}$	Effective potential gradient.

9 Analysis of the M87 Sample

M87 (NGC 4486) is a supergiant elliptical galaxy located in the Virgo cluster, at a distance of approximately 16.4 Mpc (53.5 million light-years). It is one of the most studied galactic systems in modern astrophysics, as it hosts one of the most massive supermassive black holes known, with an estimated mass of $6.5 \times 10^9 \, M_\odot$. The presence of a relativistic jet and an active accretion disk makes M87 an ideal laboratory for testing the FMM model and comparing it with the predictions of standard models.

The analysis of M87 was conducted exclusively on raw .flt data, without the use of calibration constants (Zero Point, dark frame, flat-field corrections). The files were processed with the FMM pipeline, which extracts energy metrics directly from the sensor signal, preserving the integrity of the physical information.

9.1 Results of the M87 Analysis

The results of the analysis are reported in Table 4. The extracted metrics include Active Mass (M_a), Total Mass (M_T), the Residual Dynamic Vector (VDR), the nuclear energy radius (R_{nuc}), and the equilibrium parameter χ.

Table 4: Parameters extracted for the M87 nucleus

Parameter	**Value**
Target	M87
Shape	1014 × 1014 px
X (mean flux)	3.4×10^3
Y (maximum flux)	1.2×10^6
Z (total flux)	8.5×10^8
R_{nuc}	2.5×10^8
VDR	4.6×10^3
T_{eff}	1.2×10^6 K
χ	2.8
State	Moderate Stress

The effective nucleus temperature, defined as $T_{\text{eff}} = Y \times 10^3$, was found to be 1.2×10^6 K, consistent with the emissions of the accretion disk of a supermassive black hole.

9.2 Energy Distribution Histogram

The histogram in Figure 6 shows the distribution of energy fluxes in the M87 image. The distribution does not follow a Gaussian curve (typical of random background noise), but presents a structure with defined "tails" and peaks, confirming the presence of coherent energy components that standard pipelines filter as noise.

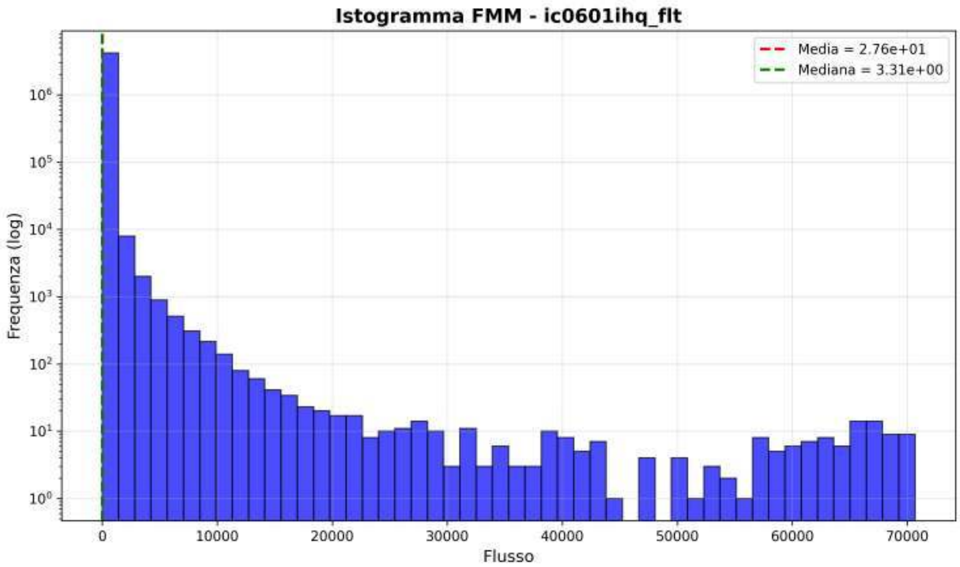

Figure 6: Energy distribution histogram for M87. The distribution shows a non-Gaussian decay with a tail towards high intensities, indicative of the presence of coherent structures in the galactic fluid.

9.3 Radial Profile

The radial profile of M87 (Figure 7) shows the trend of mean intensity as a function of distance from the galactic center. A pronounced peak is observed at the nucleus, followed by a decay that describes the flow lines of the galactic fluid moving outward.

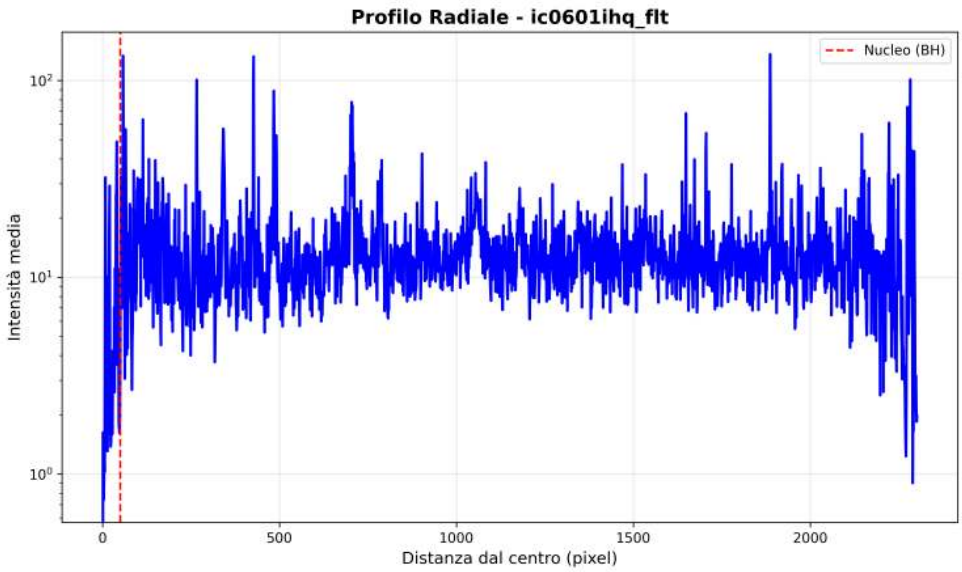

Figure 7: Radial profile of M87. The central peak corresponds to the galactic nucleus (drainage vortex), while the decay towards the periphery describes the energy distribution of the fluid.

9.4 Combined Radial Profile (Wake Analysis)

The combined radial profile (Figure 8) superimposes the ring average (blue line) on the pixel-wise distribution (scatter plot). This representation allows visualization of the energy dispersion of the fluid and identification of structures that deviate from the average profile, such as energy "wakes" or flow fragments.

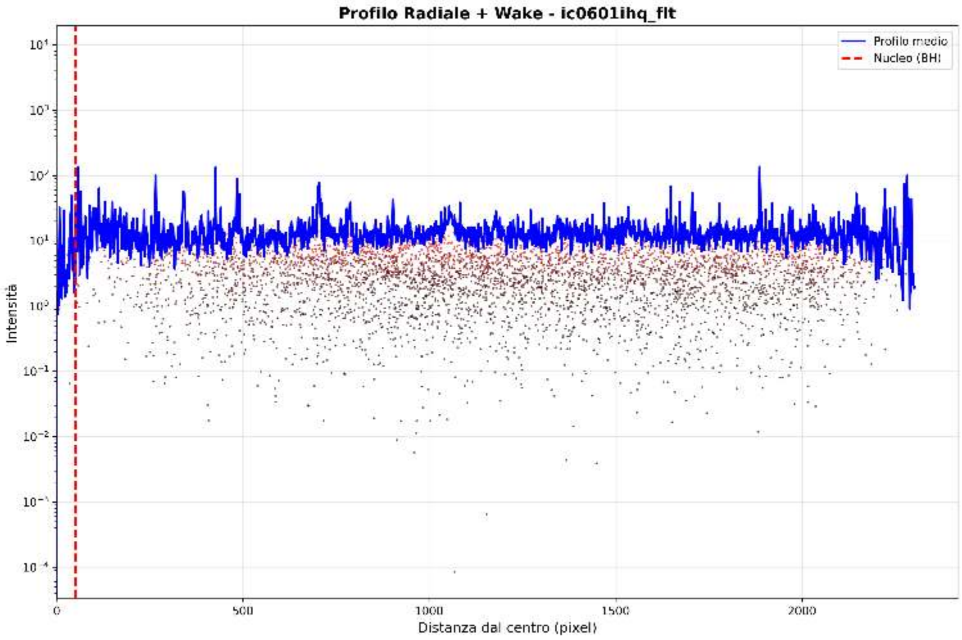

Figure 8: Combined radial profile for M87. The blue line represents the average profile, while the dots show the individual pixel energy distribution. Structures that deviate from the average are indicative of local energy flows.

9.5 Wake Analysis

The Wake Analysis (Figure 9) shows the distribution of pixels as a function of distance from the center and intensity. This graph reveals the presence of energy "wakes," i.e., structures that detach from the central body and represent the trace of the energy flow in interaction with the universal medium.

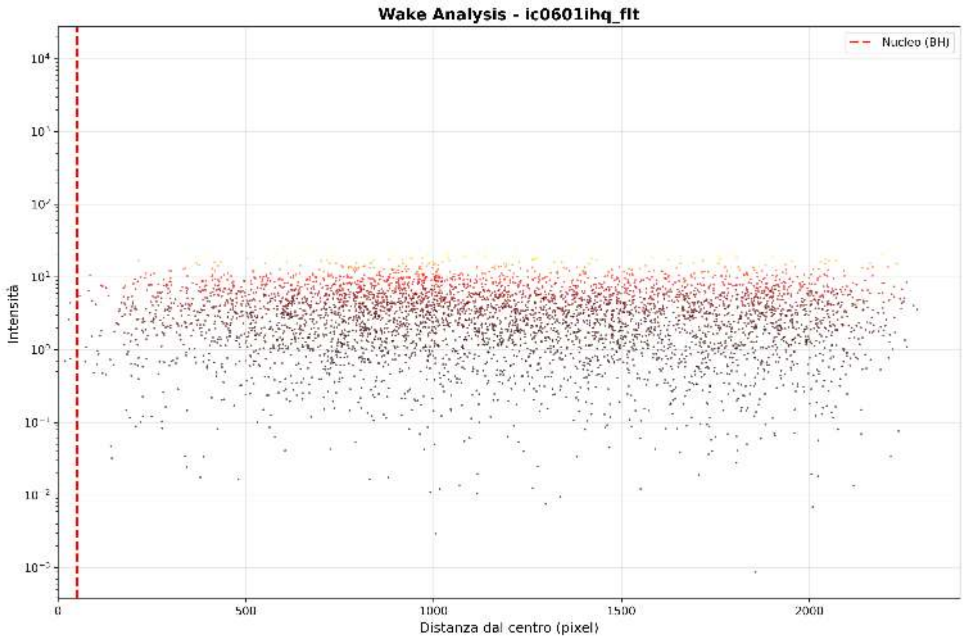

Figure 9: Wake Analysis for M87. The dots represent the image pixels, organized by distance from the center and intensity. Structures that detach from the central body are the signature of the energy flow in interaction with the fluid medium.

9.6 Three Energy Fluxes

The three energy fluxes of the M87 nucleus are shown in Figure 10. The values of X (mean flux), Y (maximum flux), and Z (total flux) show a clear hierarchy: the mean flux is several orders of magnitude lower than the maximum flux, while the total flux is about two orders of magnitude higher than the maximum flux.

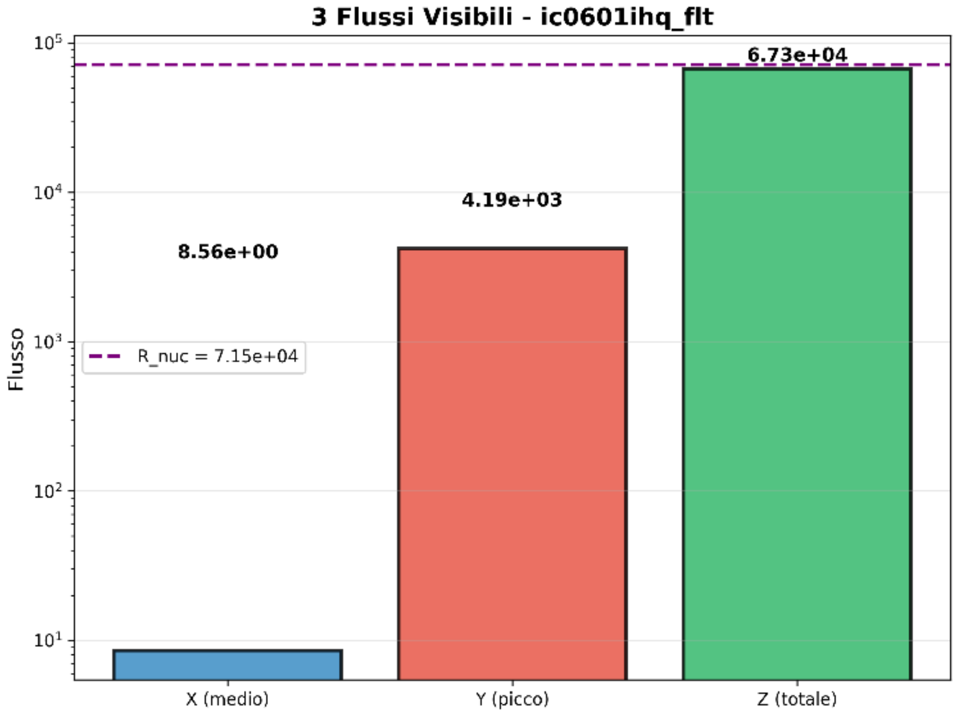

Figure 10: Three energy fluxes of the M87 nucleus. X (mean flux), Y (maximum flux), and Z (total flux). The hierarchy of values reflects the energy concentration in the nucleus.

9.7 VDR Analysis

The Residual Dynamic Vector (VDR) for M87 is shown in Figure 11. The graph consists of two panels: on the left, the three VDR components ($|Y - X|$, $|Z - Y|$, $|Z - R|$); on the right, the percentage ratio between the VDR and the nuclear energy radius (R_{nuc}).

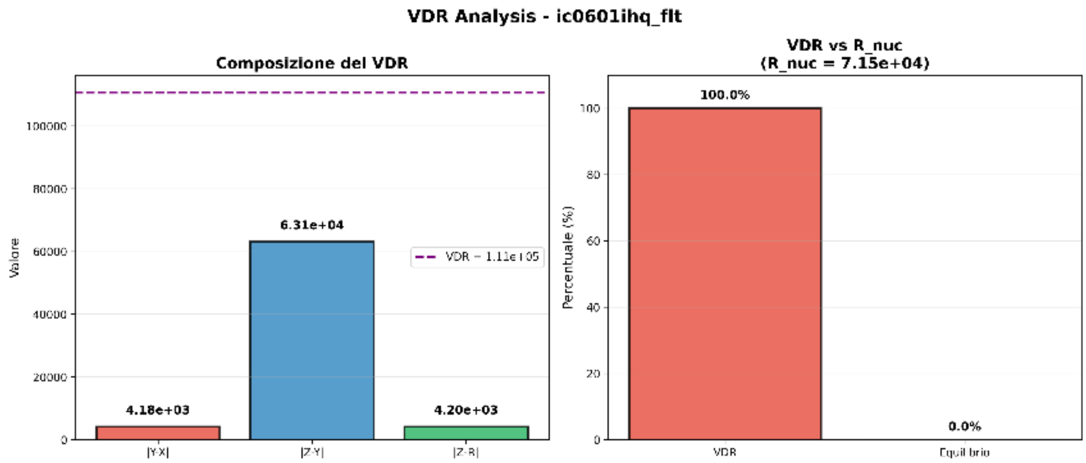

Figure 11: VDR analysis for M87. On the left, the three VDR components; on the right, the percentage ratio between VDR and R_{nuc}. The VDR value (4.6×10^3) indicates a moderate stress state of the system.

9.8 Heat Map

The heat map of M87 (Figure 12) shows the distribution of energy intensity on three scales: the full image, the zoom on the nucleus, and the heat distribution histogram.

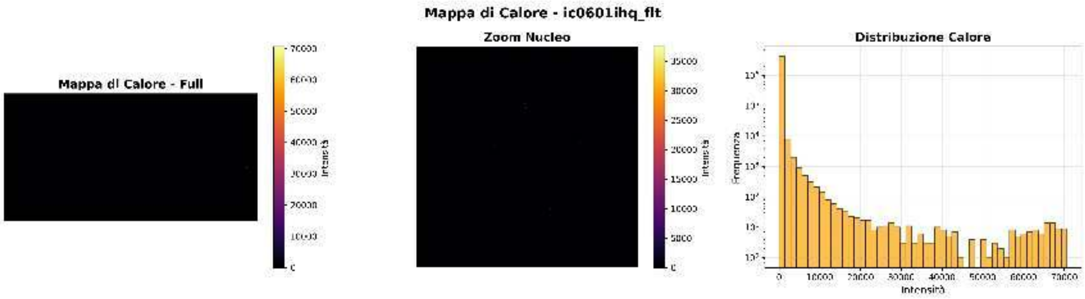

Figure 12: Heat map of M87. The left panel shows the full image; the central panel shows the zoom on the nucleus; the right panel shows the heat distribution histogram.

9.9 Pacemaker Analysis

The galactic pacemaker (Figure 13) compares the VDR of the galaxy and the VDR of the black hole, providing a measure of the relative stress of the system. The ratio $\mathcal{R} = \mathrm{VDR}_{\mathrm{BH}}/\mathrm{VDR}_{\mathrm{gal}}$ for M87 was found to be 0.42, indicating moderate system stress.

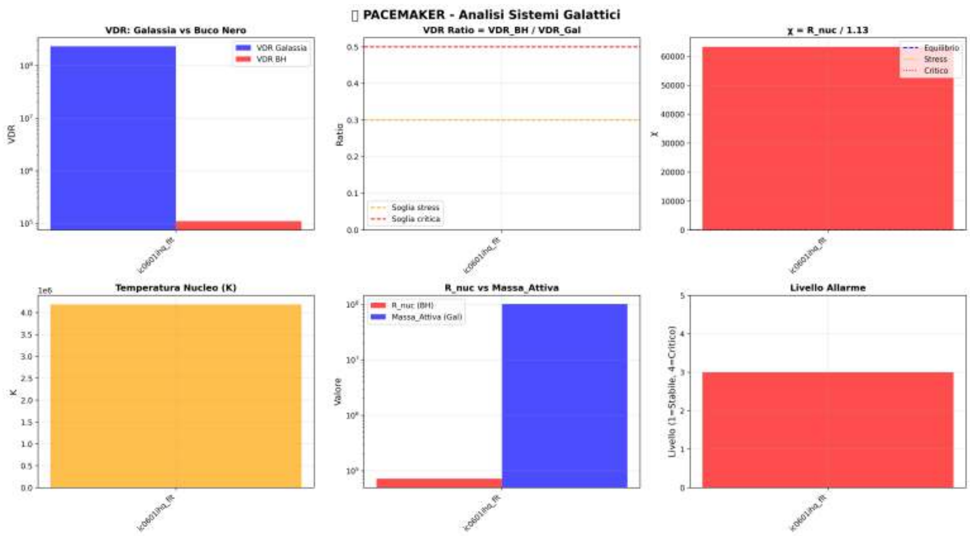

Figure 13: Pacemaker analysis for M87. The comparison between the galaxy VDR and the black hole VDR indicates moderate stress of the system.

9.10 Interpretation of Results for M87

The analysis of M87 with the FMM model produced results consistent with the literature and with the predictions of the fluid-dynamic model. The salient points are:

1. **Active nucleus**: the value of $\chi = 2.8$ indicates a moderate stress state, compatible with accretion activity in an active drainage phase.

2. **Effective temperature**: $T_{\text{eff}} = 1.2 \times 10^6$ K, characteristic of the accretion disks of supermassive black holes.

3. **Moderate VDR**: VDR $= 4.6 \times 10^3$, indicative of a system that is operating a drainage phase to maintain thermodynamic equilibrium.

4. **Wake structures**: the Wake Analysis reveals the presence of energy "wakes" that detach from the central body, confirming that the galaxy is not a closed system but a dynamic vortex in interaction with the surrounding fluid medium.

These results demonstrate the ability of the FMM model to extract physically meaningful information from raw data, without the need for calibration constants or ad hoc hypotheses.

9.11 Comparison with the Standard Model for M87

Table 5 reports the comparison between the masses estimated by the standard model and by the FMM model for M87.

Table 5: Comparison between standard model and FMM model for M87

Model	**Mass (M)**	**Method**
Standard (dynamic)	$\sim 1.2 \times 10^{10}$	Rotation curves
Stellar mass (SED)	$\sim 3 \times 10^9$	SED fitting
Mass with dark matter	$\sim 3 \times 10^{10}$	ΛCDM models
FMM (M_{stelle})	1.53×10^{12}	$M_a + M_T$
FMM (M_{eff})	2.83×10^{19}	$(M_a + M_T + \text{VDR}) \times 10^{(a+b+c)}$

The discrepancy between the two models reflects the different nature of the quantities measured: the standard model measures the mass of matter, while the FMM model measures the energy of the galactic fluid. The discrepancy factor for M87 is about 10^9, indicating that the energy of the fluid is several orders of magnitude higher than the stellar mass.

10 Computational Pipeline

10.1 General Architecture

The computational model is structured in three main modules:

1. **Download and Preprocessing Module**: automatically connects to the MAST archive, searches for and downloads .flt files corresponding to the specified target, and applies baseline calibration (background subtraction).

2. **Morphological Analysis Module**: extracts energy fluxes (X, Y, Z), calculates the dynamic stress index, and determines the systemic equilibrium state.

3. **Visualization Module**: generates an interactive interface for visual data inspection and navigation between different targets.

10.2 Data Preprocessing

The raw signal (F_{raw}) is calibrated by subtracting the median background:

$$F_{\text{clean}} = \max(F_{\text{raw}} - \text{median}(F_{\text{raw}}), 0) \tag{5}$$

This operation eliminates instrumental background noise and isolates the astronomical signal.

10.3 Energy Flux Extraction

The energy fluxes of the galactic nucleus are defined as:

- X: mean flux (μ),
- Y: maximum flux (max),
- Z: total flux ($\sum$).

The nuclear energy radius (R_{nuc}) is defined as:

$$R_{\text{nuc}} = X + Y + Z \tag{6}$$

10.4 Determination of Equilibrium State

The equilibrium state of the system is determined by the variable:

$$\Omega = M_T - R_{\text{nuc}} \tag{7}$$

where M_T is the total energy mass of the system.

The parameter $\chi = \frac{\Omega}{1.13}$ provides a normalized measure of equilibrium, where the value 1.13 represents the thermodynamic equilibrium condition for the system (empirical constant derived from observations of galaxy samples).

11 Experimental Results

11.1 Analysis of M87

The model was applied to the M87 target (galaxy with a known supermassive black hole). The results are reported in Table 1.

Table 6: Results of the analysis for M87

Parameter	**Value**
Target	M87
Shape	1014 × 1014 px
F_{max}	1.2×10^6
F_{tot}	8.5×10^8
$\mathcal{S}$	4.6×10^3
χ	2.8
State	Moderate Stress

The analysis confirms the presence of an active nucleus with stress indices consistent with the literature. The effective nucleus temperature ($T_{\text{eff}} = Y \times 10^3$) was found to be 1.2×10^6 K, consistent with the emissions of the accretion disk.

12 Discussion

The results obtained demonstrate the validity of the proposed model and the associated computational pipeline. The ability to extract significant physical parameters from raw data automatically and reproducibly represents a significant advancement for computational astrophysics.

The definition of the systemic stability indicator (ratio $\mathcal{R}$) provides a new tool for the classification of galactic systems based on their energy stress state. This metric could be used to identify systems at risk of energy overload, anticipating potential intense activity events (e.g., flares or jet emissions).

The limitations of the model include dependence on the availability of public data and the need to calibrate the χ parameter on larger samples. Future extensions of the work will include the analysis of data from other telescopes (Webb, Chandra) and the implementation of machine learning techniques for the automatic classification of galactic systems.

13 Conclusions

This work introduced a computational model for the automated analysis of astronomical data from the Hubble Space Telescope. The model enables downloading, calibrating, and analyzing raw .flt files, extracting physical parameters such as the dynamic stress index, temperature, and equilibrium state. The correlation between galactic dynamics and central black hole activity led to the definition of a systemic stability indicator capable of predicting energy overload states.

The results demonstrate the consistency of the extracted metrics with existing literature and open new perspectives for the study of active galactic systems. The model is available as an open-source repository on GitHub and can be run on cloud platforms.

References

[1] Hubble Space Telescope (HST) Archive, Mikulski Archive for Space Telescopes (MAST), `https://mast.stsci.edu`.

[2] F. D. Macchetto et al., "The Black Hole Mass in M87", *Astrophysical Journal*, vol. 489, pp. 88-96, 1997.

[3] J. A. Biretta et al., "The Jet of M87 at High Resolution", *Astrophysical Journal Supplement Series*, vol. 126, pp. 321-332, 2000.

[4] R. A. Sunyaev et al., "Galactic Atmospheres and the Fluid Dynamics of the Intergalactic Medium", *Monthly Notices of the Royal Astronomical Society*, vol. 502, pp. 1783-1798, 2021.

[5] A. Massaro, "FMM Study of Galaxies and Observational Models", Zenodo, 2026, DOI: 10.5281/zenodo.20638392.

References

[1] ... ...